frontiers | Frontiers in Materials

TYPE Original Research
PUBLISHED 22 June 2023
DOI 10.3389/fmats.2023.1214873

OPEN ACCESS

EDITED BY
Chaoqun Dang,
Zhejiang University, China

REVIEWED BY
Licong An,
Purdue University, United States
Xiaobin Feng,
Wuhan University of Technology, China

*CORRESPONDENCE
Youzhi Lin,
youzhi-lin@outlook.com

RECEIVED 30 April 2023
ACCEPTED 12 June 2023
PUBLISHED 22 June 2023

CITATION
Zhong M and Lin Y (2023), Area effect during the fracture process of high-Niobium-Titanium-Aluminum alloys under continuous tension loading-unloading.
Front. Mater. 10:1214873.
doi: 10.3389/fmats.2023.1214873

Area effect during the fracture process of high-Niobium-Titanium-Aluminum alloys under continuous tension loading-unloading

Mingjie Zhong[1] and Youzhi Lin[1,2]*

[1]Zhanjiang University of Science and Technology, Zhanjiang, China, [2]Artie McFerrin Department of Chemical Engineering, Texas A&M University, College Station, TX, United States

Based on the extracted results of the continuous tension loading-unloading testing, and observations of the corresponding cracks and fracture surfaces for the high-Niobium-Titanium-Aluminum alloys, both tensile damage and fracture mechanism were systematically studied. From the acquired results, it was demonstrated that the continuous tension loading-unloading did not affect the elastic modulus of the alloy. However, it decreased in fracture stress, fracture strain, and fracture work per unit area, and increased in irreversible strain. This result shows that the irreversible strain is not mainly caused by the volume effect of microcracks, but by the plastic strain of the materials. Although the density of the micro-cracks produced by multi-loading and unloading was small, most of the micro-cracks were concentrated on a certain section area, which results in an obvious area effect caused by the damage of the microcrack. In addition, the further propagation of the main crack under lower re-loading stress was not caused by the application of higher normal stress but by the residual tensile stress, which depends on the deterioration of the material at the crack tip during the unloading process of the alloy. These small amounts of microcracks are usually concentrated on the cross-sectional area, and the area effect caused by the microcracks damage is also obvious, which leads to a reduction of the fracture performance. Therefore, the area effect ultimately induces a decrease in fracture stress.

KEYWORDS

high-Niobium-Titanium-Aluminum alloys, tension loading-unloading, area effect, fracture stress, damage mechanism

Introduction

High Nb-TiAl alloys have excellent high-temperature mechanical properties with low densities, and they are regarded as the best candidate materials for the turbine blades used in gas turbines and aircraft engines (Lin et al., 2011; Imayev et al., 2021). The addition of Nb can significantly improve the creep and oxidation resistance of TiAl alloys (Ding et al., 2018). Compared with conventional Titanium alloys, the density of TiAl alloys is about 15% lower. Nevertheless, the high-temperature tolerance of the high Nb-TiAl alloys is twice that of the conventional titanium alloys (Wang et al., 2020a; Wang et al., 2020b; LIN et al., 2022). Moreover, compared with the traditional Nickel-based superalloys, the mass of the high Nb-TiAl alloys with the same volume is smaller than half in the temperature range of

600°C–850°C (CAO et al., 2018). High Nb-TiAl alloys have also many comparative advantages, such as low density, high specific strength, good toughness, and good creep resistance. Thus, they are considered potential materials for replacing Titanium alloys and Nickel-base super alloys for aerospace applications (Bewlay et al., 2016; Guyon et al., 2016). However, the application of TiAl-based alloys is restricted due to their poor ductility at room temperature and intrinsic brittleness as an intermetallic compound.

The addition of Nb may improve the mechanical properties and ductility of the TiAl-based alloys at room temperature by refining the grains, whereas a trace quantity of boron may also improve the ductility of the TiAl-based alloys (Hu et al., 2012; Vorobjova et al., 2020). Therefore, TiAl-based alloys are considered a new generation of materials with broad development prospects in the field of aerospace.

At present, there are many works in the literature on the damage and fracture of TiAl-based alloys under static loading (Lin et al., 2014; Cui et al., 2016; Xu et al., 2019). Along these lines, Makoto Hasegawa found that the deformation constraints at grains play major roles in the local damage behaviour of the TiAl-based alloys (Hasegawa et al., 2019). The TiAl possesses high tensile strength and good tensile elongation due to the anomalous strengthening behaviour of the intermetallic layers, as well as the presence of the multilayer interfaces (Shen et al., 2018; Gong et al., 2021a; Schnabel and Scheider, 2021; Yu et al., 2022). The crack initiation and propagation are directly related to the applied load, deflection, and acoustic emission events, while the crack tends to propagate along the precipitated phases and the lamellar interface (Feng et al., 2017; Lapin et al., 2018; Wang et al., 2018). J. Lapin found the important influence of coarse carbide particles on the crack initiation and propagation mechanism of the high Nb-TiAl alloys and the residual strains (Lapin et al., 2019). Additionally, various factors for improving the crack tip plasticity and fracture toughness were investigated (Appel et al., 2018). A combination of the microscopic toughening mechanisms including crack deflection, shear ligaments, plasticity, and microcracking significantly contributes to the toughness of the TiAl-based alloys (Liu et al., 2017; Sun et al., 2018; Zhu et al., 2018).

However, the impact of micro-damage and macro-properties of the TiAl-based alloys change after performing repeated loading and unloading has been scarcely reported in the literature. Besides, it is not clear how exactly the damage in the previous stage affects the damage in the subsequent stage. Under this direction in this work, the underlying damage mechanism of the high Nb-TiAl alloys was further studied by performing continuous tension and unloading experiments, which provides a solid theoretical basis for the design and application of engineering components composed of high Nb-TiAl alloys.

Materials and methods

The high Nb-TiAl alloy that was used in this experiment was formed after 1 h of vacuum heat treatment of less than 0.1 Pa at the temperature value of 1,300°C and cooled with furnace. Its chemical composition is shown in Table 1.

The plate specimens that were cut by using the CKX-2AJ wire electrical discharge machine (WEDM) are shown in Figure 1. The length of the specimens in Figure 1 is 70 mm, the width is 10 mm, and the thickness is 2 mm. All samples have undergone mechanical polishing and surface inspection to ensure that there are no cracks or other defects on the surface before conducting tensile testing on the specimens. Microstructure of the high Nb-TiAl alloy is shown in Figure 2. A number of short rods of boride cross the lamellae can be seen (Kartavykh et al., 2014; Li et al., 2018; Huo et al., 2023). Under the room temperature and load-controlled loading mode, the specimens were unloaded under different applied stress values on the INSTRON-1341 test machine, which is manufactured by American Instron Engineering Corporation and then were unloaded under the pre-specified load. By gradually increasing the unloaded stresses, after repeating the tension and unloading processes many times, the specimen was finally tensile fracture.

The load-displacement curves during loading and unloading were automatically recorded by the testing machine. After the application of the same continuous tension, the other batch of specimens does not break the specimens in the final stage. However, the specimens were unloaded under the corresponding load in the final unloading stage. Then, the surface and internal structures of the specimens unloaded under different loads were observed by using an JSM6700F scanning electron microscope (SEM), which is manufactured by Japan Electronics Co., Ltd. From the acquired images, it was proven that the surface and internal cracks determine the damage parameters, whereas the

TABLE 1 Chemical compositions of the high Nb-TiAl alloys.

C&E	Al	Nb	Hf	Si	B	Ti
wt%	44	8.0	2.0	0.2	1.0	Bal

Note: C&E, Chemical element; wt%, Weight percent; Bal, Banlance.

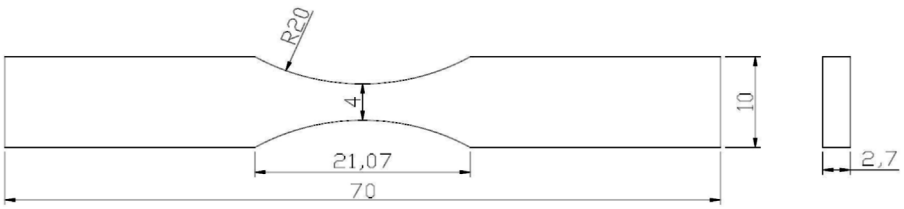

FIGURE 1
Shape of the continuous tensile and unloading specimens (The unit is mm).

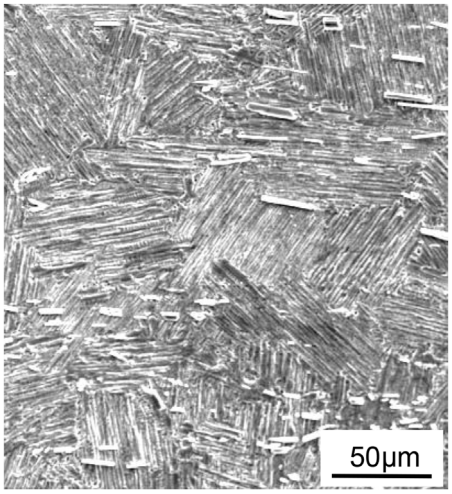

FIGURE 2
Microstructure of the high Nb-TiAl alloy.

impact of the damage parameters on the final mechanical properties of the material was also thoroughly investigated.

The fracture morphology of the specimen after tension unloading was observed by SEM imaging, and the initial and final fractured parts were determined during the preloading procedure. The area along the surface and the river grain were systematically analysed. At the same time, this area was associated and analysed by taking into account the fracture morphology and the surface crack.

Results and discussion

Data analysis of the continuous tensile unloading test for the high Nb-TiAl alloys

The macroscopic experimental results of the multiple tension and unloading process obtained in this experiment are shown in Tables 2, 3. The crack densities (π) in Table 3 were obtained by observing the SEM of the sample surface during the loading-unloading process, as shown in Figure 3, and counting the number of cracks on each sample surface. Whereas some corresponding macroscopic curves are depicted in Figure 4.

Figure 4A illustrates the stress-strain curves of the specimen SN04 after stretching to 41.78 MPa, 81.75 MPa, 159.76 MPa, 324.21 MPa, and continuously loading-unloading- loading until breaking. As can be observed, the tensile and unloading paths coincide basically when the specimen undergoes unloading stress before the value of 159.76 MPa, indicating that no obvious irreversible strain exists. At this time, there is also no obvious change in the fracture stress of the specimen. When specimen SN04 is stretched to the value of 324.21 MPa, a small irreversible strain is observed, and the fracture stress begins to show a decreasing trend. Figure 4B displays the stress-strain curve of

TABLE 2 Results of the continuous tension and unloading test for the high Nb-TiAl alloys.

No.	S_e/mm^2	σ_{ui}/MPa						σ_f/MPa
		σ_{u1}	σ_{u2}	σ_{u3}	σ_{u4}	σ_{u5}	σ_{u5}	
SN01	3.98*1.88	40.96						549.72
SN02	4.02*1.95	40.14	80.19					535.29
SN03	4.00*2.01	39.89	79.25	160.36				517.74
SN04	3.96*1.92	41.87	81.75	159.76	324.21			513.88
SN05	4.02*1.98	40.93	80.53	160.43	321.45	401.32		482.64
SN06	4.00*1.99	41.43	80.72	161.77	320.94	395.20	442.23	467.03

Note: No, Specimen number; S_e, Effective area of original cross-section in the specimen's ligament; σ_{ui}, Unloading stress, and 'i' is the order of unloading; σ_f, Fracture stress.

TABLE 3 Analysis of the cracks in the high Nb-TiAl alloys after continuous tension and unloading.

No.	S_e/mm^2	σ_{ui}/MPa						π/(strip/mm^2)
		σ_{u1}	σ_{u2}	σ_{u3}	σ_{u4}	σ_{u5}	σ_{u6}	
SN07	4.04*1.96	40.65						12.76
SN08	4.00*1.92	41.28	80.23					17.23
SN09	4.04*1.94	39.86	81.49	160.25				26.52
SN10	4.00*1.92	41.74	80.35	161.62	319.45			32.86
SN11	3.98*2.00	40.15	79.27	160.55	320.73	402.61		28.75
SN12	4.02*1.94	41.33	80.84	159.54	319.03	393.14	436.04	30.68

Note: No, Specimen number; S_e, Effective area of original cross-section in the specimen's ligament; σ_{ui}, Unloading stress, and 'i' is the order of unloading; π, crack fracture density.

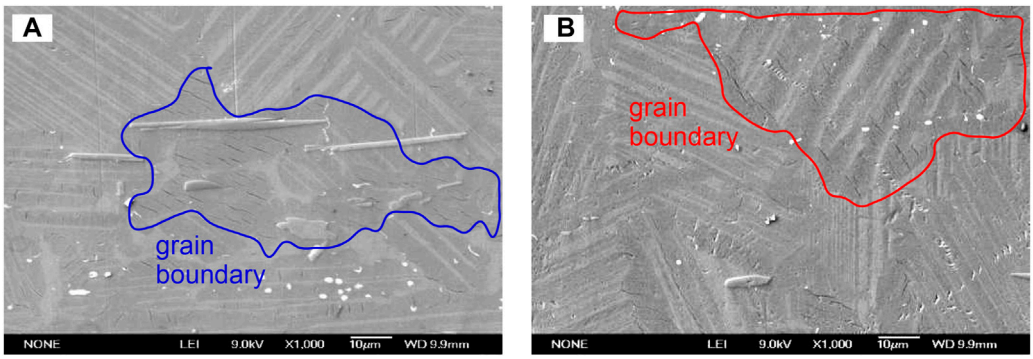

FIGURE 3
Surface of the high Nb-TiAl alloy tensile-unloaded specimens: **(A)** sample SN11 at 320.73 MPa, **(B)** sample SN12 at 319.03 MPa.

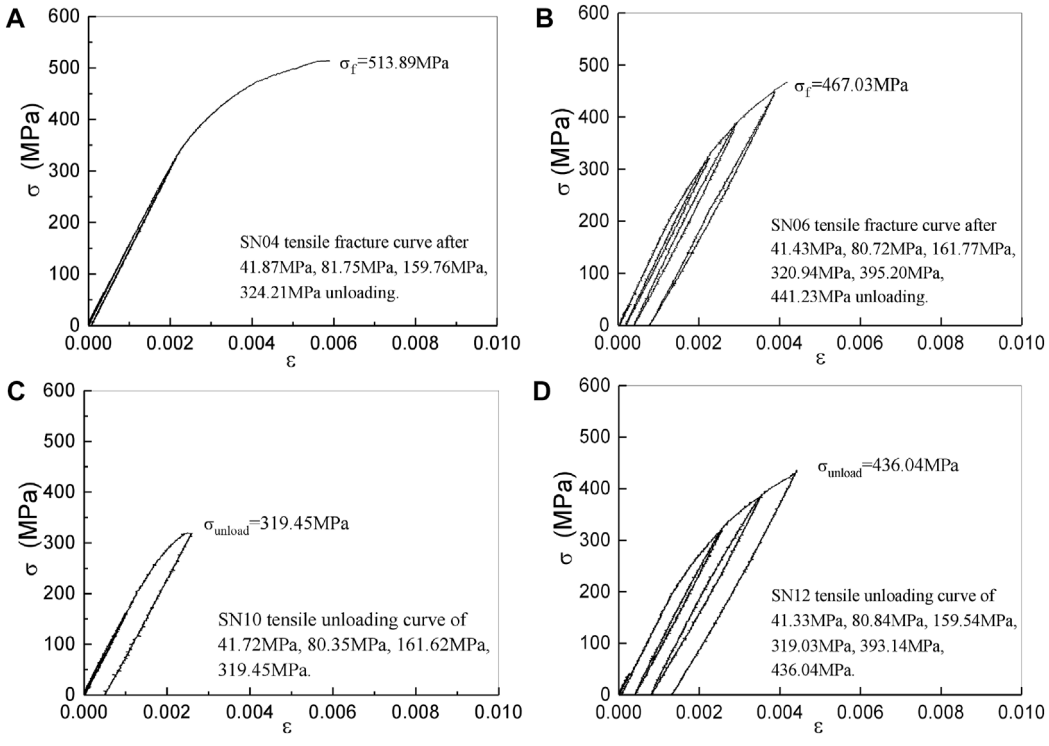

FIGURE 4
Stress-strain curve of the continuous tension loading and unloading of samples SN04 **(A)**, SN06 **(B)**, SN10 **(C)**, and SN12 **(D)**.

the sample SN06 after performing the same continuously stretching and unloading of the sample SN04 by stretching to the value of 442.23 MPa and unloading, and then stretching to the fracture. Figure 4B depicts that the irreversible strain occurs when the specimen is unloaded after stretching to the value of 442.23 MPa, and the residual strain after the unloading process is about 0.001, at which time the fracture stress is decreased significantly. Figure 4C presents the stress-strain curve of the sample SN10 after enforcing the strain values of 41.72 MPa, 80.35 MPa, 161.62 MPa, and continuous tension unloading process and then unloading at the strain value of 319.45 MPa. Figure 4D shows the stress-strain curve of the specimen SN12 unloaded at the values of 436.04 MPa after the implementation of the 41.33 MPa, 80.84 MPa, 159.54 MPa, 319.03 MPa, 393.14 MPa stress loads, and then the continuous tensile unloading process was applied. As can be observed from Figures 4C, D, if a microcrack occurs in the material, it will not propagate under small stress values but will propagate only when it

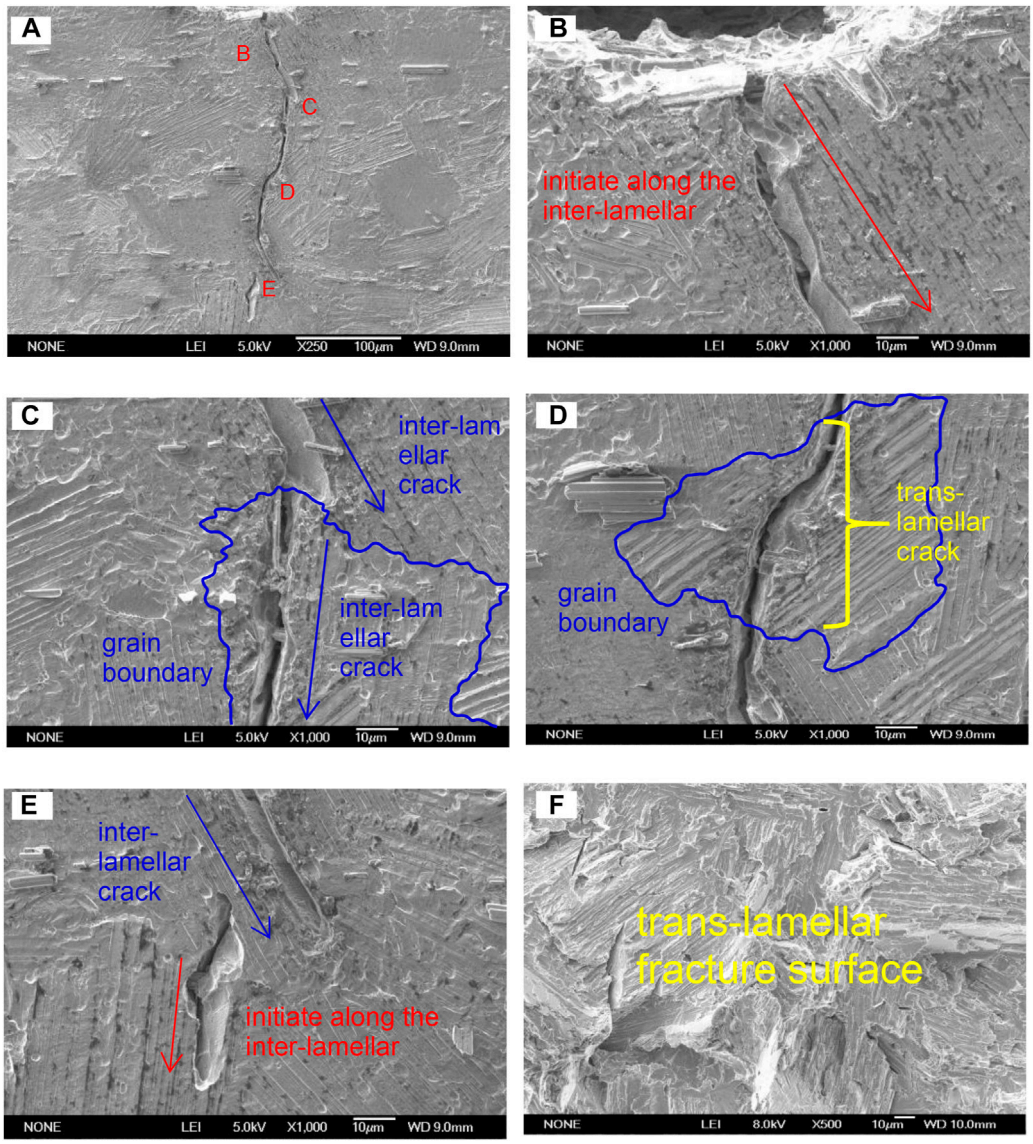

FIGURE 5
Sample surface and fracture surface of the high Nb-TiAl alloy tensile-unloaded: **(A~E)** sample SN10 at 319.45 MPa, **(F)** fracture surface of the sample SN12.

is stretched to the unloading stress. The cracks generated before unloading will not propagate during their unloading process. Only after unloading to zero and reloading to the unloading stress can the crack further propagate. At this point, the crack will be longer than when it was first loaded to the unloading stress. This situation can be observed during the tensile test.

By combining the extracted outcomes reported in Tables 2, 3; Figure 4, it was found that the elastic modulus of the TiAl-based alloy remained unchanged regardless of the application of numerous tension and unloading cycles. The fracture stress, fracture strain, and fracture work per unit area hardly changed before the unloading stress was below the value of 159.76 MPa. When the unloading stress was higher than the value of 159.76 MPa, these macro-performance indicators decreased significantly. Hence, it can be argued that the material will not be damaged until a certain unloading stress value is reached (CAO, 2006; CAO, 2020). On top of that, the damage does not affect the elastic modulus of the material (Li et al., 2004; Bonora et al., 2011).

Fracture surfaces analysis of the high Nb-TiAl alloy continuous tension unloading specimens

The micro-crack characteristics of the TiAl-based alloy under the application of continuous tension and unloading are shown in Figure 5, whereas the calculation of the number of micro-cracks is shown in Table 3. The B, C, D, and E in Figure 5A correspond to the four figures in Figures 5B–E. Figure 5 depicts that most of the

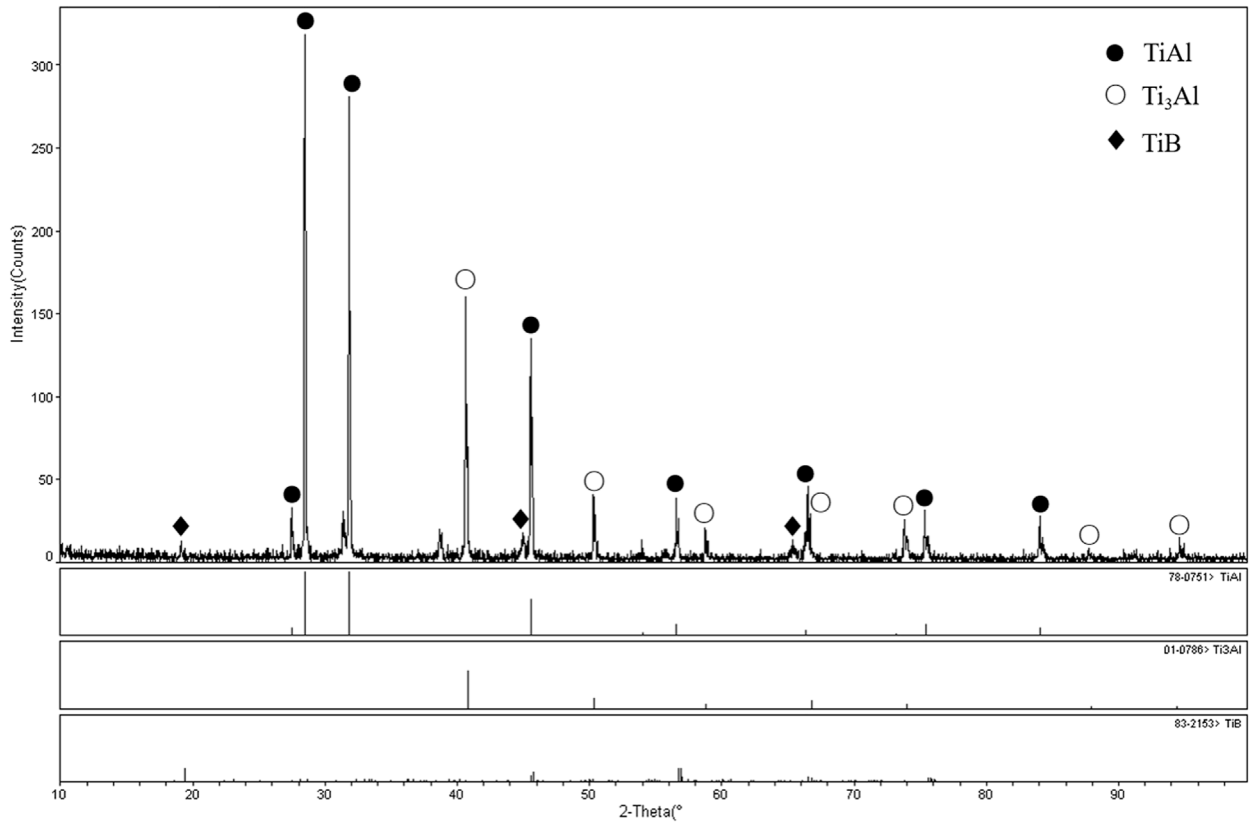

FIGURE 6
XRD pattern of SN12 tensile-unloaded specimen.

microcracks initiate and propagate along the inter-lamellar direction, as shown in Figures 5B, E. The size of the microcracks is also closely related to the size of the layer clusters, and the generated microcracks by stretching are also related to the direction of the inter-lamellar and stretching axes, as shown in Figure 5A. The origins of this effect are associated with the fact that normal stress is considered the main driving force for the initiation and expansion of a microcrack in the material, while the inter-lamellar strength is much lower than that of the trans-lamellar strength.

Previous reports in the literature have found that the crack initiation and propagation processes are not only dependent on the relative orientation of the layer and the stretching axis but also can be affected by the grain boundary orientation (Zhang et al., 2020; Gong et al., 2021b; Guo et al., 2022; Peng et al., 2023). Therefore, after unloading under different loading stress values, most of the observed microcracks were inter-lamellar cracks, as shown in Figure 5C. As far as the plate tension specimens are concerned, because the stress was basically uniform in the range of the gauge, the crack initiation will take place in the most advantageous weak inter-lamellar crack, which is the area where the applied stress is easiest to reach the stress of the crack initiation. Thus, when the applied loading stress is relatively small, a large number of inter-lamellar cracks will be observed, as shown in Figures 5B, C, E.

With the increase in the unloading stress, a small number of trans-lamellar cracks will appear, as shown in Figure 5D. Finally, the specimen will fracture when the applied stress is reached, where most trans-lamellar cracks appear, as shown in Figure 5F. As can be seen from Table 3; Figure 5, the number of cracks does not increase with the increase of the unloading stress, and the length of the cracks does not increase with the increase of unloading stress.

The composition analysis was conducted on the position of the fracture zone in the middle of the sample arc, and the XRD diffraction pattern is shown in Figure 6. In the fracture zone rich in boride, the main components are TiAl, Ti3Al, and TiB, and other components are not highlighted in the XRD diffraction pattern due to low content. According to the crystal orientation and microstructure of boride, the elongated microstructure in Figure 5 is TiB. Most boride were distributed along the tensile axis at the boundary of the cluster, that is, perpendicular to the normal stress direction, which had a certain blocking effect on the crack growth and played a toughening role to a certain extent. This result proves that with the increase in the unloading stress, no damage increasing trend was found in using microcracks to characterize material damage.

Figure 7 illustrates the fracture morphology of the sample SN04 after performing loading-unloading cycles. More specifically, Figure 7A shows that a crack initiation area appeared on the left side of the fracture surface, whereas the enlargement of these surfaces is shown in Figure 7B. This area

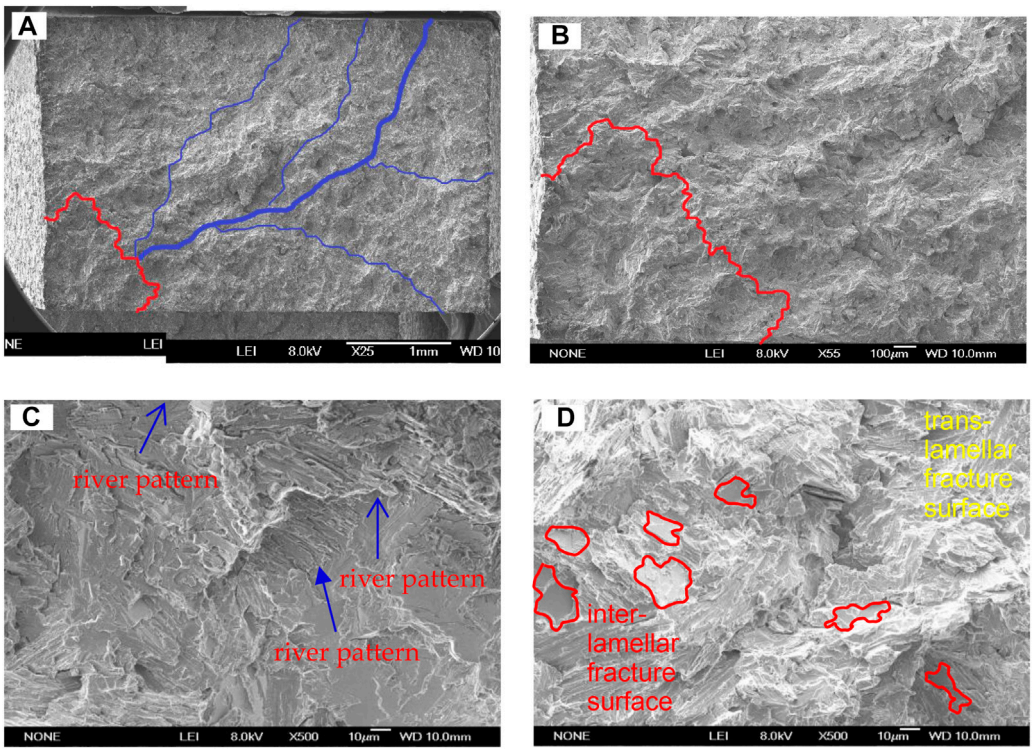

FIGURE 7
Fracture surface of the high Nb-TiAl alloy specimen SN04 in the tensile: **(A)** full view of fracture surface, **(B)** crack initiation area, **(C)** river pattern and fracture direction, and **(D)** trans-lamellar fracture and inter-lamellar fracture surface.

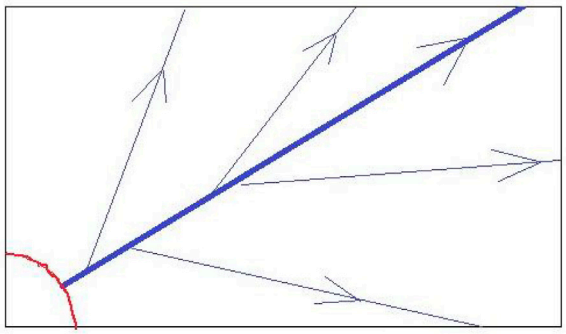

FIGURE 8
Fracture process of the high Nb-TiAl alloys tensile specimen.

is composed of many small inter-lamellar surfaces, where no obvious river pattern can be detected. When the specimen is loaded to a high stress, a Griffiths crack source of a certain size is first generated at the weak internal structure of a material near its maximum stress section, and then quickly propagates towards multiple favorable orientations, inducing cleavage fracture of the entire sample, as shown in Figure 8.

Some inter-lamellar surfaces were generated during the implementation of the loading process before the fracture. From left to right, the whole specimen presents several cleavage planes with obvious river pattern trend, as shown in Figure 7C, which were formed when the crack passed through the residual section of the specimen at the final fracture. The orientation of the river pattern in Figure 7C is basically consistent with the fracture direction shown in Figure 8. On the entire fracture surface, the main surface is trans-lamellar fracture, with only a small portion of the inter-lamellar fracture surface being found, as shown in Figure 7D. The red area in the bottom left corner of Figure 8 is the initiation zone, the thick blue line is the main fracture path, and the thin blue line is the secondary fracture path. Therefore, the non-directional inter-lamellar surfaces and the directional cleavage surfaces on the fracture surface can be qualitatively regarded as the main criterion for crack formation during the loading-unloading cycles or at the final fracture.

As can be ascertained from Figures 5–7, after the loading, unloading and reloading processes, the material's modulus of elasticity on the stress-strain curve of tensile fracture has not changed, and no decrease was observed. This outcome indicates that the volume effect caused by microcrack damage is not obvious since the increased rate of the applied stress remains basically unchanged when the specimen is continuously loaded. Additionally, at a relatively fast loading rate, there is not enough time for the formation of microcracks. In the high Nb-TiAl alloys, the surface density of microcracks becomes bigger with the increase of the stress during the loading-unloading process, but the trend is not obvious. The grain size of the whole layer structure of these materials is also smaller, which limits the volume effect caused by the generation microcracks. At the same time, because the stress of the whole plate material is basically uniform, the generated micro-cracks are closely related to the orientation of the layer and the grain size.

Hence, there is no trend that the micro-cracks increase obviously with the increase of the unloading stress.

Microcracks sometimes do not appear before the final fracture in the continuous tension loading-unloading of the high Nb-TiAl alloys. Therefore, no obvious drop curve in the stress-strain curve is recorded. In this case, the difference in the number and length of the microcracks caused by the implementation of the different preloading and different loading processes cannot be compensated in the final loading process. This result shows that different preloading and different loading processes have some impact on fracture stress. For the plate tension test, some micro-cracks were firstly generated on the weakest surface under the application of a small load, and micro-cracks were continuously generated with continuous tension.

When the applied stress reached a certain level, the density of microcracks will be increased obviously, and many microcracks will appear on one of the weak surfaces. This result indicates that the area effect caused by the micro-crack damage of the high Nb-TiAl-based alloy is obvious. With the increase in the applied stress, the micro-cracks on the weak surface will connect with each other, while brittle fracture will occur at the same time. Therefore, the fracture morphology only shows some inter-lamellar and trans-lamellar surface, and the early cracking takes place generally in a small inter-lamellar surfaces. Of course, there will be a few obvious river patterns on the final fracture surface. However, the proportion of the river pattern area is very small.

In the future, studies on the influence of damage of this material on its engineering service life can be carried out. It was suggested to strengthen the safety and reliability analysis of its materials for practical application. Under the condition of ensuring certain reliability, it is suggested to expand the application of this material in relevant industrial fields.

Conclusion

From the analysis of the continuous cyclic loading-unloading test of the high Nb-TiAl alloy, it deeply studied the damage evolution process of the material, and improved the theory of fracture mechanics. Some main conclusions were as follows:

1) The volume effect caused by microcrack damage was not obvious, and the area effect caused by microcrack damage was very obvious. Although the density of the micro-cracks produced by multi-loading and unloading was small, most of the micro-cracks were concentrated on a certain section area, which results in an obvious area effect caused by the micro-crack damage of the high Nb-TiAl-based alloy. This leads to a decrease in the fracture properties. The test indicated that the area effect ultimately leads to a decrease in the fracture stress.
2) The volume effect caused by microcrack damage was not obvious. This result shows that the irreversible strain is not mainly caused by the volume effect of microcracks, but by the plastic strain of the materials, i.e., the irreversible strain during loading-unloading-reloading including a large number of plastic strains and a small number of strains caused by microcracks. The fracture stress of the high Nb-TiAl alloy decreased after conducting repeated cyclic loading and larger unloading stress cycles, and the fracture strain and fracture work per unit area began to decrease, while the irreversible strain gradually increased.
3) It was demonstrated that the elastic modulus of the material is not affected by performing repeated tensile loading-unloading cycles.
4) Boride have a certain blocking effect on the crack growth and play a toughening role to a certain extent.
5) The further propagation of the main crack is not caused by the application of higher normal stress but by the residual tensile stress under the lower re-loading stress of the high Nb-TiAl alloy. Therefore, the further propagation of the main crack under lower re-loading stress strongly depends on the deterioration of the material at the crack tip during the unloading process.

Data availability statement

The original contributions presented in the study are included in the article/Supplementary Material, further inquiries can be directed to the corresponding author.

Author contributions

MZ: conceptualization, methodology, validation, and writing-original draft; YZ: conceptualization, investigation, resources, and writing and editing. All authors contributed to the article and approved the submitted version.

Funding

YL had been funded in part by the Texas A&M University and the China Scholarship Council. This work was supported by the National Natural Science Foundations of China [Grant No. 50471109] and the Natural Science Foundation of Zhejiang Provincial of China (No. GF20E080010).

Conflict of interest

The authors declare that the research was conducted in the absence of any commercial or financial relationships that could be construed as a potential conflict of interest.

Publisher's note

Supplementary material

The Supplementary Material for this article can be found online at: https://www.frontiersin.org/articles/10.3389/fmats.2023.1214873/full#supplementary-material

References

Appel, F., Paul, J. D. H., Peter, S., Oehringa, M., Kolednikb, O., Predanc, J., et al. (2018). The effect of residual stresses and strain reversal on the fracture toughness of TiAl alloys. *Mater. Sci. Eng. A* 709 (1), 17–29. doi:10.1016/j.msea.2017.10.010

Bewlay, B. P., Nag, S., Suzuki, A., and Weimer, M. J. (2016). TiAl alloys in commercial aircraft engines. *Mater. A. T. High. Temp.* 33 (4-5), 549–559. doi:10.1080/09603409.2016.1183068

Bonora, N., Ruggiero, A., Gentile, D., and De Meo, S. (2011). Practical applicability and limitations of the elastic modulus degradation technique for damage measurements in ductile metals. *Strain* 47, 241–254. doi:10.1111/j.1475-1305.2009.00678.x

Cao, H. (2020). *Deformation and fracture mechanism of single crystal γ-TiAl*. Lanzhou, China: Lanzhou University of Technology.

Cao, R. (2006). *Study on damage and fracture behavior of γ-TiAl based slloys*. Lanzhou, China: Lanzhou University of Technology.

Cao, Z.-H., Sun, Y., Zhi-peng, W. A. N., Ren, L., and Lian-xi, H. U. (2018). Development of critical damage model of TiAl alloy during hot deformation. *Chin. J. Nonferrous Metals* 28 (4), 670. doi:10.19476/j.ysxb.1004.0609.2018.04.04

Cui, N., Wang, X.-P., Kong, F.-T., Chen, Y.-Y., and Zhou, H.-T. (2016). Microstructure and properties of a beta-solidifying TiAl-based alloy with different refiners. *Rare Met.* 35 (1), 42–47. doi:10.1007/s12598-015-0634-y

Ding, J., Zhang, M., Liang, Y., Ren, Y., Dong, C., and Lin, J. (2018). Enhanced high-temperature tensile property by gradient twin structure of duplex high-Nb-containing TiAl alloy. *Acta Mater.* 161, 1–11. doi:10.1016/j.actamat.2018.09.007

Feng, G., Li, Z., Feng, S., and Zhang, W. (2017). Microstructure evolution and formation mechanism of laser-ignited SHS joining between C_f/Al composites and TiAl alloys with Ni-Al-Ti interlayer. *Rare Met.* 36 (9), 58. doi:10.1007/s12598-015-0542-1

Gong, X., Chen, R. R., Wang, Y., Su, Y. Q., Guo, J. J., and Fu, H. Z. (2021a). Microstructure and oxidation behavior of NiCoCrAlY coating with different Sm2O3 concentration on TiAl alloy. *Front. Mater.* 8, 710431. doi:10.3389/fmats.2021.710431

Gong, Z., Jin, W., Sun, W., Wang, L., and Ke, X. (2021b). Effects of B and Y additions on the microstructure and tensile behaviour of high-Nb TiAl alloys. *Rare Metal Mater. Eng.* 50 (08), 2760–2764.

Guo, S., Li, X., Dong, K., Gu, J., Zhou, Q., and Wang, K. (2022). Microstructure and shear property of high-temperature brazing of TiAl alloy and 316L stainless steel with a Ni-based amorphous filler. *Front. Mater.* 9, 1098397. doi:10.3389/fmats.2022.1098397

Guyon, J., Hazotte, A., Wagner, F., and Bouzy, E. (2016). Recrystallization of coherent nanolamellar structures in Ti48Al2Cr2Nb intermetallic alloy. *Acta Mater.* 103, 672–680. doi:10.1016/j.actamat.2015.10.049

Hasegawa, M., Inui, T., and Dlouhý, I. (2019). Effect of heat treatment at (β+γ) Two phase region on fracture toughness in TiAl intermetallic compound. *Mater. Sci. Eng. A* 748 (3), 21–26. doi:10.4028/www.scientific.net/kem.810.21

Hu, D., Yang, C., Huang, A., Dixon, M., and Hecht, U. (2012). Grain refinement in beta-solidifying Ti44Al8Nb1B. *Intermetallics* 23, 49–56. doi:10.1016/j.intermet.2011.12.022

Huo, J., He, B., and Lan, L. (2023). Effects of boron on microstructure and mechanical properties of high-Nb TiAl alloy fabricated via laser melting deposition. *J. Materi Eng Perform*. doi:10.1007/s11665-023-07851-3

Imayev, V. M., Ganeev, A. A., Trofimov, D. M., JuParkhimovich, N., and Imayev, R. M. (2021). Effect of Nb, Zr and Zr + Hf on the microstructure and mechanical properties of β-solidifying γ-TiAl alloys. *Mater. Sci. Eng. A* 817, 141388. doi:10.1016/j.msea.2021.141388

Kartavykh, A. V., Gorshenkov, M. V., Tcherdyntsev, V. V., and Podgorny, D. A. (2014). On the state of boride precipitates in grain refined TiAl-based alloys with high Nb content. *J. Alloys Compd.* 586 (1), S153–S158. doi:10.1016/j.jallcom.2013.03.104

Lapin, J., Štamborská, M., Kamyshnykova, K., Pelachováa, T., Klimováa, A., and Bajana, O. (2018). Fracture behaviour of cast *in-situ* TiAl matrix composite reinforced with carbide particles. *Mater. Sci. Eng. A* 721 (4), 1–7. doi:10.1016/j.msea.2018.02.077

Lapin, J., Štamborská, M., Kamyshnykova, K., Pelachová, T., Klimová, A., and Bajana, O. (2019). Room temperature mechanical behaviour of cast *in-situ* TiAl matrix composite reinforced with carbide particles. *Intermetallics* 105 (2), 113–123. doi:10.1016/j.intermet.2018.11.007

Li, M., Xiao, S., Chen, Y., Xu, L., and Tian, J. (2018). The effect of boron addition on the high-temperature properties and microstructure evolution of high Nb containing TiAl alloys. *Mater. Sci. Eng. A* 733, 190–198. doi:10.1016/j.msea.2018.07.019

Li, T., Grignon, F., Benson, D. J. K., Olevsky, E. A., Jiang, F., Rohatgi, A., et al. (2004). Modeling the elastic properties and damage evolution in Ti–Al3Ti metal–intermetallic laminate (MIL) composites. *Mater. Sci. Eng. A* 374 (1–2), 10–26. doi:10.1016/j.msea.2003.09.074

Lin, J. P., Zhao, L. L., Li, G. Y., Zhang, L. Q., Song, X. P., Ye, F., et al. (2011). Effect of Nb on oxidation behavior of high Nb containing TiAl alloys. *Intermetallics* 19 (2), 131–136. doi:10.1016/j.intermet.2010.08.029

Lin, Y., Fu, G., and Cao, R. (2014). Compression damage and fracture Behaviors of γ-TiAl based alloys. *Chin. J. Rare metals* 38 (2), 334. doi:10.13373/j.cnki.cjrm.2014.02.024

Lin, Y., Liao, P., Fu, G., and Chen, J. (2022). Damage and fracture mechanism of full lamellar high Nb-TiAl alloy. *Ordnance Material Sci. Eng.* 45 (4), 8–12. doi:10.14024/j.cnki.1004-244x.20220412.002

Liu, N., Zhou, L., Xu, W., Wang, Y., Zhang, G., and Yuan, H. (2017). Hot deformation behavior and microstructural evolution of powder metallurgical TiAl alloy. *Rare Met.* 36 (4), 10. doi:10.1007/s12598-016-0746-z

Peng, Y., Ye, Y., Yu, C., Wang, Z., Xu, Y., and Du, Y. (2023). Study on the preparation and performance of low-temperature sintering and high-thermal-conductivity silver nanowire film. *Metals* 13, 819. doi:10.3390/met13040819

Schnabel, J. E., and Scheider, I. (2021). Crystal plasticity modeling of creep in alloys with lamellar microstructures at the example of fully lamellar TiAl. *Front. Mater.* 7, 581187. doi:10.3389/fmats.2020.581187

Shen, Z., Huang, G., He, L., Mu, R., and Li, J. (2018). Large-sized TiAl/Ti 3 Al multilayer thin sheet: Microstructures, mechanical properties and degradation mechanism. *J. Alloys Compd.* 746 (5), 102–107. doi:10.1016/j.jallcom.2018.02.097

Sun, W., Yang, F., FanKong, T., Wang, X. P., and Chen, Y. Y. (2018). Microstructure and fracture toughness of a TiAl/Ti laminated composite. *Appl. Mech. Mater.* 884 (8), 29–35. doi:10.4028/www.scientific.net/amm.884.29

Vorobjova, A., Tishkevich, D., Shimanovich, D., Zdorovets, M., Kozlovskiy, A., Zubar, T., et al. (2020). Electrochemical behaviour of Ti/Al2O3/Ni nanocomposite material in artificial physiological solution: Prospects for biomedical application. *Nanomaterials* 10, 173. doi:10.3390/nano10010173

Wang, Q., Chen, R., Yang, Y., Guo, J., Su, Y., Ding, H., et al. (2018). Effects of grain size and precipitated phases on mechanical properties in TiAl gradient materials. *Mater. Sci. Eng. A* 731 (7), 634–641. doi:10.1016/j.msea.2018.06.092

Wang, X. Y., Yang, J. R., Hu, R., Xie, M. T., Hu, D. W., and Fu, H. (2020a). Creep-induced phase instability and microstructure evolution of a nearly lamellar Ti-45Al-8.5Nb-(W,B,Y) alloy. *Acta Metallur-gica Sin.* 33, 1591–1600. doi:10.1007/s40195-020-01108-x

Wang, X., Kong, F., Cao, X., Meng-zhe, L. I. N., Zhang, C., and Chen, Y. Y. (2020b). Effect of heat treatment and thermomechanical processing on microstructure and tensile property of Ti-44Al-8Nb-0.2W-0.2B-0.5Y alloy. *China Foundry* 17 (6), 447–454. doi:10.1007/s41230-020-0097-0

Xu, R., Li, M., and Hong, L (2019). Research progress on flow behavior and constitutive models of γ-TiAl alloys deformed at elevated temperature. *Rare Metal Mater. Eng.* 48 (5), 1406.

Yu, F., Addison, O., and Davenport, A. (2022). Temperature-dependence corrosion behavior of Ti6Al4V in the presence of HCl. *Front. Mater.* 9, 880702. doi:10.3389/fmats.2022.880702

Zhang, X., Wang, H., Zhu, C., and He, W. (2020). Effect of carbon content on microstructure and mechanical properties of cast TiAl alloys. *Rare Metal Mater. Eng.* 49 (1), 138–146.

Zhu, B., Xue, X., Kou, H., Li, X., and Li, J. (2018). Effect of microstructure on the fracture toughness of multi-phase high Nb-containing TiAl alloys. *Intermetallics* 100 (9), 142–150. doi:10.1016/j.intermet.2018.06.014